AN AUTOMATED SEARCH PROCEDURE TO GENERATE OPTIMAL LOW-THRUST RENDEZVOUS TOURS OF THE SUN-JUPITER TROJAN ASTEROIDS

Jeffrey R. Stuart(1) **and Kathleen C. Howell**(2)
(1)*Graduate Student, Purdue University, School of Aeronautics and Astronautics, 701 W. Stadium Ave., West Lafayette, IN, 47907, 765-620-4342, jrstuart@purdue.edu*
(2)*Hsu Lo Professor of Aeronautical and Astronautical Engineering, Purdue University, School of Aeronautics and Astronautics, 701 W. Stadium Ave., West Lafayette, IN, 47907, 765-494-5786, howell@purdue.edu*

Abstract: *The Sun-Jupiter Trojan asteroid swarms are targets of interest for robotic spacecraft missions, and because of the relatively stable dynamics of the equilateral libration points, low-thrust propulsion systems offer a viable method for realizing tours of these asteroids. This investigation presents a novel scheme for the automated creation of prospective tours under the natural dynamics of the circular restricted three-body problem with thrust provided by a variable specific impulse low-thrust engine. The procedure approximates tours by combining independently generated fuel-optimal rendezvous arcs between pairs of asteroids into a series of coast periods near asteroids and engine operation durations between the asteroids. Propellant costs and departure and arrival times are estimated from performance of the individual thrust arcs. Tours of interest are readily re-converged in higher fidelity ephemeris models. In general, the automation procedure rapidly generates a large number of potential tours and supplies reasonable cost estimates for preliminary baseline mission design.*

Keywords: *Trojan asteroid tour, automated trajectory design, optimal low-thrust, asteroid rendezvous, variable specific impulse*

1. Introduction

Near Earth Objects (NEOs) are currently being considered for manned sample return missions,[1] while a recent NASA study assesses the feasibility of a mission to the Trojan asteroids at a New Frontiers level.[2] Tour missions within asteroid swarms allow for a broad sampling of interesting target bodies either for scientific investigation or as potential resources to support deep-space human missions. However, the multitude of asteroids within the swarms necessitates the use of automated design algorithms if a large number of potential mission options are to be surveyed. Accordingly, this investigation details a process to automatically and rapidly generate sample tours of the Sun-Jupiter L_4 Trojan asteroid swarm with a minimum of human interaction. The proposed tour creation strategy is not specific to the problem of asteroid missions and, therefore, the low-thrust tour design concept is readily applied to a diverse range of prospective mission scenarios.

High-efficiency, low-thrust propulsion systems are particularly attractive for missions to the Sun-Jupiter equilateral equilibrium points because of the relatively stable natural gravitational dynamics in these regions. Propellant-optimal, low-thrust trajectories, realized by constant specific impluse systems in nonlinear dynamical regimes, typically require coasting arcs and the careful balancing of engine capability with transfer time. The inclusion of additional coasting arcs requires engine shut-downs and restarts that may be operationally inefficient and generally infeasible. Therefore, a variable specific impulse (VSI) engine that varies the optimal thrust magnitude is selected to simplify the generation of rendezvous solutions.[3] Accordingly, no coasting arcs are required for rendezvous and the initial generation of optimal trajectories is less restrictive in terms of thrust duration. Examples of VSI engines include the Variable Specific Impulse Magnetoplasma Rocket (VASIMR) currently under development by the Ad Astra Rocket Company[4] and the Electron and Ion Cyclotron Resonance (EICR) Plasma Propulsion Systems at Kyushu University in Japan.[5]

In general, the computation of locally fuel-optimal trajectories is posed as an optimal control problem. The possible formulations to solve the problem include a low-dimension but less flexible indirect approach using optimal control theory[6, 7, 8] or a higher-dimension but more robust direct approach.[9, 10, 11] A combination of an indirect and a direct method is termed a hybrid optimization algorithm and exploits the relative benefits of both local optimization strategies. For this investigation, the Euler-Lagrange Theorem [12] offers conditions for optimal engine operation while the optimization packages SNOPT[13] and *fmincon* minimize propellant costs. Relatively short times-of-flight (compared to long-duration spiral trajectories), as well as continuation methods, further increase solution stability.

In this analysis, independently generated fuel-optimal rendezvous arcs between asteroids are automatically sequenced to create a number of candidate tours. Similar investigations have been completed by Izzo[14] and Canalias[15], though these authors implement global search algorithms that produce single tours comprised of brief flyby encounters, optimized end-to-end. In contrast, in this preliminary investigation, asteroid tours are constructed via the following process:

1. Select asteroids of interest and specify a window of opportunity.
2. Generate a number of locally optimal thrust arcs that link all possible pairs of asteroids (or a desired subset).
3. Specify an initial target asteroid as well as the available propellant mass, overall mission duration, and starting epoch.
4. Search and combine independent solution arcs to encompass all tours that satisfy the specified criteria.
5. For the available tours, estimate propellant cost, arrival and departure epochs, and time duration in the vicinity of the asteroids.
6. Select a candidate tour with desirable characteristics.
7. Transform the tour to higher fidelity models to create a continuous trajectory.

In the above procedure, Phases 2, 4, 5, and 7 are automated processes; the designer is then free to focus on the selection of the asteroids of interest, the specific mission objectives and constraints, the definition of tours of interest, and the post-processing of the results. The window of opportunity for tours is pre-specified as October 3, 2021 to October 3, 2061, that is, asteroid arrival is assumed to occur no sooner than the first date and mission operation ends at or before the latter date. For this investigation, ten asteroids with inclinations less than 5° with respect to the solar system ecliptic are selected as potential targets; Table 1 includes a list of their names. Rendezvous and fly-by opportunities with other bodies exist, but are not captured in this investigation.

The seven-step procedure employed in this study yields tours within the asteroid swarm, but a complete trajectory also requires an outbound, or interplanetary, leg that departs Earth and terminates with a rendezvous at the first asteroid in the sequence. However, for the interplanetary transfer arc

Table 1. Asteroids selected as bodies of potential scientific interest in the L_4 Trojan asteroid swarm.

Asteroid Name	
659 Nestor	5012 Eurymedon
1143 Odysseus	5652 Amphimachus
1869 Philoctetes	7152 Euneus
4057 Demophon	8241 Agrius
4138 Kalchas	8317 Eurysaces

to the swarm, more than a low-thrust propulsion system is required for this transfer to occur in a reasonable length of time. Therefore, a V_∞ at Earth departure, delivered by conventional high-thrust chemical engines, any number of planetary fly-bys, or some combination of such external options to gain energy are incorporated. After Earth departure, the only thrust along the outbound arc is delivered by the low-thrust system. This combination of low-thrust and departure V_∞ is a specific example of hybrid propulsion, i.e., the blending of various propulsion methods. By specifying that the spacecraft arrival condition matches the initial state along the tour path, the two independent segments are joined into an end-to-end baseline design offering cost and timing estimates for a Trojan asteroid tour.

2. System Models

Two key steps are initially necessary to successfully formulate the rendezvous problem, namely the definition of the physical environment to model the dynamics of the system and the construction of the initial and target state vectors. The model for the unpowered spacecraft dynamics is independent of the low-thrust and optimization strategies and is, therefore, adjusted to introduce various levels of model fidelity.

2.1 Circular Restricted Three-Body Problem

The dynamics are initially modeled in terms of the Circular Restricted Three Body Problem (CR3BP) with the Sun as one primary and Jupiter as the second. The equations of motion are formulated within the context of a rotating reference frame where $\hat{x}$ is directed from the Sun to Jupiter, $\hat{z}$ is normal to the orbital plane of the primaries and parallel to orbital angular momentum, and $\hat{y}$ completes the right-handed set. The origin of the coordinate system is the Sun-Jupiter barycenter. Incorporated into the forces that influence the motion in this system are terms that arise from the thrusting of the Variable Specific Impulse (VSI) engine. The system of equations are nondimensionalized to aid numerical integration efficiency: computed results are converted to dimensional quantities by the proper use of the characteristic quantities and spacecraft parameter values. The characteristic quantities are defined as the Sun-Jupiter distance, the mass of the primaries, the characteristic time, and the initial spacecraft mass. The spacecraft state vector is then defined as:

$$\boldsymbol{\chi} = \begin{Bmatrix} \boldsymbol{r} \\ \boldsymbol{v} \\ m \end{Bmatrix} \tag{1}$$

where $\boldsymbol{r}$ is the position vector relative to the barycenter, $\boldsymbol{v}$ is the velocity vector with respect to the barycenter as viewed by a rotating observer, and m is the instantaneous mass of the spacecraft. The equations of motion are then derived with the result:

$$\dot{\boldsymbol{\chi}} = \begin{Bmatrix} \dot{\boldsymbol{r}} \\ \dot{\boldsymbol{v}} \\ \dot{m} \end{Bmatrix} = \begin{Bmatrix} \boldsymbol{v} \\ \boldsymbol{f}_n(\boldsymbol{r},\boldsymbol{v}) + \frac{T}{m}\boldsymbol{u} \\ -\frac{T^2}{2P} \end{Bmatrix} \tag{2}$$

where T is thrust magnitude, P is engine power, $\boldsymbol{u}$ is a unit vector defining the thrust direction, and $\boldsymbol{f}_n$ represents the natural acceleration of the spacecraft. Furthermore, denote the six-dimensional vector that includes position $\boldsymbol{r}$ and velocity $\boldsymbol{v}$ by the vector $\boldsymbol{x}$, where $\boldsymbol{x} = \left[x\, y\, z\, \dot{x}\, \dot{y}\, \dot{z}\right]^T$. The scalar elements of $\boldsymbol{f}_n$ are then expressed in terms of the rotating frame as:

$$\boldsymbol{f}_n = \begin{Bmatrix} 2\dot{y} + x - \frac{(1-\mu)(x+\mu)}{d_1^3} - \frac{\mu(x+\mu-1)}{d_2^3} \\ -2\dot{x} + y - \frac{(1-\mu)y}{d_1^3} - \frac{\mu y}{d_2^3} \\ -\frac{(1-\mu)z}{d_1^3} - \frac{\mu z}{d_2^3} \end{Bmatrix} \tag{3}$$

where d_1 and d_2 are the distances to the vehicle from the Sun and Jupiter, respectively, that is

$$d_1 = \sqrt{(x+\mu)^2 + y^2 + z^2} \tag{4}$$

$$d_2 = \sqrt{(x+\mu-1)^2 + y^2 + z^2}. \tag{5}$$

The mass parameter μ is

$$\mu = \frac{M_J}{M_S + M_J} \tag{6}$$

where M_S and M_J are the masses of the Sun and Jupiter, respectively. The power P is defined as a scalar value between zero and a maximum available power level specified by the engine model, such that

$$0 \leq P \leq P_{\max}. \tag{7}$$

Then, the engine thrust T is evaluated via

$$T = \frac{2P}{I_{sp} g_0} \tag{8}$$

where I_{sp} is the engine specific impulse and $g_0 = 9.80665$ m/s^2, the gravitational acceleration at the surface of the Earth. Further information on the system and spacecraft parameters is available in Table 2.

2.2 Point-Mass Ephemeris Model and Relative Equations of Motion

While the CR3BP serves as a powerful tool for initial analysis, higher fidelity models are required for more detailed and accurate investigation. A more accurate model for point masses moving under the influence of gravity is provided by the relative vector equation of motion for a particle i moving with respect to a central body q:

$$\ddot{\boldsymbol{r}}_{qi} + \frac{G(m_i + m_q)}{r_{qi}^3}\boldsymbol{r}_{qi} = G \sum_{\substack{j=1 \\ j \neq i,q}}^{n} m_j \left(\frac{\boldsymbol{r}_{ij}}{r_{ij}^3} - \frac{\boldsymbol{r}_{qj}}{r_{qj}^3} \right) \tag{9}$$

Table 2. System and spacecraft parameter values.

Quantity	Value
Solar mass (M_S), kg	1.9891×10^{30}
Jupiter mass (M_J), kg	1.8986×10^{27}
Gravitational Constant (G), $\frac{\text{km}^3}{\text{kg}\cdot\text{sec}^2}$	6.67428×10^{-20}
Mass parameter (μ)	9.53816×10^{-4}
Sun-Jupiter distance (l^*), km	7.78412×10^{8}
Characteristic Time (t^*), sec	5.95911×10^{7}
Characteristic Time (t_d^*), days	6.89712×10^{2}
Reference spacecraft mass (m_r), kg	500
Maximum engine power ($P_{\max}$), kW	1.0

where additional bodies are denoted by the subscript j. The positions and velocities of celestial bodies are available from the Jet Propulsion Laboratory's HORIZONS system[16]. The relative position vector $\boldsymbol{r}_{ij}$ is defined

$$\boldsymbol{r}_{ij} = \boldsymbol{r}_{qj} - \boldsymbol{r}_{qi} \tag{10}$$

where all positions are known relative to the central body q. Therefore, the natural dynamics of the spacecraft in an inertial frame are mathematically modeled as

$$\boldsymbol{f}_n(t, \boldsymbol{r}_{qi}) = -\frac{G(m_i + m_q)}{r_{qi}^3}\boldsymbol{r}_{qi} + G\sum_{\substack{j=1\\ j\neq i,q}}^{n} m_j\left(\frac{\boldsymbol{r}_{ij}}{r_{ij}^3} - \frac{\boldsymbol{r}_{qj}}{r_{qj}^3}\right) \tag{11}$$

where the system is no longer time invariant. Since motion within the asteroid swarm is relatively distant from most perturbing bodies, only the Sun and Jupiter are incorporated in the ephemeris model for this preliminary investigation. Additional bodies can be readily included and the number does not alter the low-thrust engine model and the implementation of the optimization algorithm.

2.3 Initial and Target States

The computation of rendezvous arcs requires the definition of an initial state from which the spacecraft departs whenever a thrust segment is initiated and a target state that serves as a matching condition for the spacecraft state vector upon arrival. This definition is accomplished by specifying the initial state $\boldsymbol{x}_I$ to be the position and velocity of a specified asteroid (or Earth, for the Earth to asteroid arc) that is considered the departure body for a particular rendezvous segment. Likewise, the target state $\boldsymbol{x}_T$ is the position and velocity of the desired arrival body. In the ephemeris point-mass model in Section 2.2, the states of celestial bodies at a given epoch are determined by interpolation of the HORIZONS data. For the simplified model presented in Section 2.1, however, an equivalent continuous path for the celestial body is determined, where the motion satisfies the natural dynamics from the Sun-Jupiter CR3BP. Accordingly, a set of reference nodes are extracted from the HORIZONS data, transformed to the Sun-Jupiter rotating frame, and supplied as the initial guess for a multiple shooting corrections process where continuity is specified for all interior points.[17] In this corrections scheme, the nodes are allowed to vary without constraint, so long as the resulting solution provides a continuous path for the asteroid motion. Figure 1 displays one such conversion, with the original HORIZONS data represented by a dashed line and the reconverged continuous CR3BP trajectory the solid line. Motion for all 10 asteroids, as well as the Earth, is transitioned to the CR3BP. Once a tour trajectory is determined within the context of the CR3BP, the results are transitioned to the point-mass ephemeris model to restore the true positions of the asteroids and the Earth.

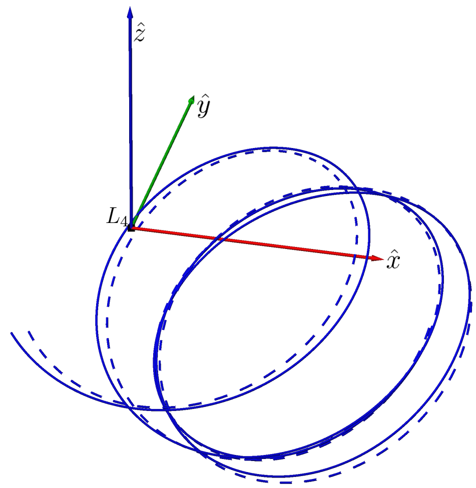

Figure 1. Path of asteroid 1143 Odysseus from Oct. 3, 2021 to Oct. 3, 2061 in Sun-Jupiter rotating frame from ephemeris data (dashed) and under CR3BP dynamics (solid)

3. Trajectory Optimization

A local hybrid optimization scheme is proposed wherein indirect procedures are combined with direct methods to retain low-dimensionality and, therefore, computational efficiency, while increasing the robustness of the process convergence characteristics. The application of techniques from the calculus of variations supplies conditions on optimal operation of the engine while requiring only the solution of an initial set of co-states. In addition to reducing the number of function evaluations per iteration, this indirect approach also ensures smooth and continuous control history while not restricting engine operation time histories to an assumed form. A spacecraft mass objective function is locally optimized using a gradient based procedure, removing a requirement to derive and employ the sensitive transversality conditions of indirect methods. Global and heuristic algorithms, though not addressed in this study, can also be used to optimize fuel performance.

3.1 Indirect Optimization

For optimal thrust performance, the rendezvous problem is first posed indirectly using the calculus of variations for a formulation as a two-point boundary value problem (2PBVP). The engine operational states are then determined from the Euler-Lagrange equations. However, the thrust duration TD must be pre-specified when a VSI engine is employed. If no limit is placed on either the thrust duration or mass consumption, the optimization process drives TD and I_{sp} to infinity for zero propellant mass.

To fully define the optimization problem, the performance index and the boundary conditions must also be specified. To arrive at the target asteroid with the maximum final spacecraft mass for a specified thrust duration, the performance index J is defined

$$\max J = m_f. \tag{12}$$

The boundary conditions and the Hamiltonian are adjoined to the performance index, so that Eq. (12) is expanded to become the Bolza function

$$\max J' = m_f + \boldsymbol{\nu}_0^T \boldsymbol{\psi}_0 + \boldsymbol{\nu}_f^T \boldsymbol{\psi}_f + \int_{t_0}^{t_f} [H - \boldsymbol{\lambda}^T \dot{\boldsymbol{\chi}}] dt \tag{13}$$

where H is the problem Hamiltonian, $\boldsymbol{\lambda}$ is a co-state vector, the terms $\boldsymbol{\psi}$ are vectors comprised of boundary conditions, and the vector terms involving $\boldsymbol{\nu}$ are Lagrange multipliers corresponding to the boundary conditions. The co-state vector is then

$$\boldsymbol{\lambda} = \begin{Bmatrix} \boldsymbol{\lambda_r} \\ \boldsymbol{\lambda_v} \\ \lambda_m \end{Bmatrix} \tag{14}$$

where $\boldsymbol{\lambda_r}$ and $\boldsymbol{\lambda_v}$ are three-dimensional vectors comprised of the position and velocity co-states, respectively, and the scalar λ_m is the mass co-state. The initial and final vector boundary conditions are

$$\boldsymbol{\psi}_0 = \boldsymbol{x}_I - \boldsymbol{x}_I(\tau_0) = \mathbf{0} \tag{15}$$

and

$$\boldsymbol{\psi}_f = \boldsymbol{x}_T - \boldsymbol{x}_T(\tau_0 + TD) = \mathbf{0} \tag{16}$$

where the subscripts I and T indicate the states associated with the current asteroid and target asteroid, respectively. Equation (15) is implicitly satisfied by defining $\boldsymbol{x}_I$ as the state along the current asteroid trajectory as defined by the parameter τ_0. The final, or target, boundary conditions in Eq. (16) are satisfied by solving the boundary value problem.

The calculus of variations is employed to define several properties of the 2PBVP and acquire the derivatives of the co-states. The problem Hamiltonian is

$$H = \boldsymbol{\lambda}^T \dot{\boldsymbol{\chi}} = \boldsymbol{\lambda}_r^T \boldsymbol{v} + \boldsymbol{\lambda}_v^T \left[\boldsymbol{f}_n(\boldsymbol{r}, \boldsymbol{v}) + \frac{T}{m} \boldsymbol{u} \right] - \lambda_m \frac{T^2}{2P} \tag{17}$$

where the value of H is constant over the trajectory. The optimal controls emerge by maximizing the Hamiltonian with respect to the controls T, P, and $\boldsymbol{u}$ such that

$$P = P_{\max} \tag{18}$$

$$T = \frac{\lambda_v P_{\max}}{\lambda_m m} \tag{19}$$

$$\boldsymbol{u} = \frac{\boldsymbol{\lambda_v}}{\lambda_v} \tag{20}$$

where λ_v=$||\boldsymbol{\lambda_v}||$. Given these control expressions, the Hamiltonian is reformulated and Eq. (17) is rewritten as

$$H = \boldsymbol{\lambda}_r^T \boldsymbol{v} + \boldsymbol{\lambda}_v^T \boldsymbol{f}_n + S \cdot T \tag{21}$$

where S is the switching function

$$S = \frac{\lambda_{\boldsymbol{v}}}{m} - \frac{\lambda_m T}{2P_{\max}}. \tag{22}$$

The Euler-Lagrange conditions for optimality modify the performance index in Eq. (13). With the reformulated Hamiltonian, that is, Eq. (21), the following equations of motion for the co-states emerge

$$\dot{\boldsymbol{\lambda}} = -\left(\frac{\partial H}{\partial \boldsymbol{\chi}}\right)^T = \left\{ \begin{array}{c} -\boldsymbol{\lambda}_{\boldsymbol{v}}^T \left(\frac{\partial \boldsymbol{f}_n}{\partial \boldsymbol{r}}\right) \\ -\boldsymbol{\lambda}_{\boldsymbol{r}}^T - \boldsymbol{\lambda}_{\boldsymbol{v}}^T \left(\frac{\partial \boldsymbol{f}_n}{\partial \boldsymbol{v}}\right) \\ \lambda_{\boldsymbol{v}} \frac{T}{m^2} \end{array} \right\} \tag{23}$$

where the initial state for λ_m is set to unity to reduce the number of variables to be determined. Note that: (a) a similar procedure to minimize the initial mass for a given target mass provides identical conditions for engine operation, and (b) the differential equations for the co-states do not change form based upon the underlying natural dynamics; thus, $\frac{\partial \boldsymbol{f}_n}{\partial \boldsymbol{r}}$ and $\frac{\partial \boldsymbol{f}_n}{\partial \boldsymbol{v}}$ can be freely substituted when using models of varying fidelity.

3.2 Hybrid Optimization and Hybrid Propulsion

The design process for the overall mission trajectory is divided into two parts. The creation of the tour within the asteroid swarm is first accomplished; computation of individual rendezvous arcs is an integral component. The second step is then the generation of the interplanetary arc from Earth to the asteroid swarm. This split is used advantageously to isolate and address challenges for each of the two components without affecting the design and computation of the opposite element. However, the end conditions of the outbound segment must be carefully blended with the initial conditions of any specifice rendezvous sequence. Therefore, it is natural to pose the propellant minimization problem differently for the two components, the outbound segment and the tour phase. So, for rendezvous arcs within the swarm, the initial spacecraft mass is specified as the reference mass from Table 2, i.e., $m_0 = m_r$. The optimization package SNOPT is then used to maximize the final mass m_f, with the additional non-linear constraints specified by Eqs. (15) and (16). Note that the same initial condition $m_0 = m_r$ is used for all independently generated asteroid to asteroid arcs.

As previously stated, the Earth departure leg greatly benefits from the inclusion of a hybrid propulsion scheme assuming an initial departure velocity is allowed. Propellant mass is optimized by targeting a final spacecraft mass of $m_f = m_r$ while using SNOPT to minimize the spacecraft mass at Earth departure m_0. However, the inclusion of a departure velocity invalidates the initial boundary condition as posed in Eq. (15). Position continuity must be maintained, but velocity is now constrained, i.e.,

$$\sqrt{\Delta\boldsymbol{v}_I \cdot \Delta\boldsymbol{v}_I} - V_\infty = 0 \tag{24}$$

where $\Delta\boldsymbol{v}_I = \boldsymbol{v}_I - \boldsymbol{v}_\oplus(\tau_0)$, such that $\boldsymbol{v}_I$ is the spacecraft initial velocity and $\boldsymbol{v}_\oplus(\tau_0)$ is defined as the velocity of Earth at spacecraft departure. The departure V_∞ is selected based upon the capabilities of a chemical booster stage or hyperbolic velocity after an Earth fly-by. Thus, for the interplanetary leg, SNOPT minimizes the initial spacecraft mass m_0 subject to the constraints given in Eqs. (16) and (24) and position continuity with the Earth at the initial departure epoch.

4. Automated Tour Creation

A mission to the vicinity of the Sun-Jupiter "Greek" or "Trojan" asteroid families will almost certainly entail rendezvous with and the observation of multiple objects. Recall that the asteroid tour is determined prior to the generation of an Earth-to-asteroid outbound segment. A strategy is proposed to rapidly and automatically generate a large number of candidate asteroid tours satisfying a set of constraints. This trajectory evaluation scheme yields only approximate propellant costs and is, therefore, intended solely for preliminary design analysis. However, overall performance comparisons can be assessed and specific trajectory concepts are readily transitioned to higher fidelity models that offer more accurate estimates of propellant consumption. The construction of rendezvous sequences within the swarm occurs in two steps: (a) the computation of sets of asteroid-to-asteroid arcs and (b) the constrained selection and ordering of thrust intervals. Both phases benefit from automation.

4.1 Rendezvous Arc Detection and Computation

For even a relatively small number of asteroids, manually determining and generating all possible optimal rendezvous arcs is a laborious process. For example, for any given pair of asteroids, there are several epochs over the specified 40-year window that define a locally optimal departure state for a rendezvous arc. So, when all possible asteroid pairs are considered, there are hundreds of locally-optimal rendezvous arcs for any given thrust duration TD. Therefore, an automated scheme that detects conditions amenable to locally optimal transfers and, subsequently, computes the corresponding point solutions is critical for rapid trajectory design.

Conditions likely to yield optimal transfers include low distance and low relative velocity between asteroids. Several detection algorithms to identify such conditions with a large set of feasible transfer options were explored. The most efficient method strategy searches epochs for those that correspond to the minimum relative distance between an asteroid pair. Thus, solutions to the local optimization problem

$$\min d_a(\tau_0) = \|\boldsymbol{r}_T(\tau_0) - \boldsymbol{r}_I(\tau_0)\| \tag{25}$$

supply the initial guesses for the parameter τ_0 in the rendezvous problem. Thus, the problem involves only one free parameter, and a grid search readily produces all the solutions over the 40-year window of opportunities. Once the set of initial parameters τ_0 are determined, the hybrid optimization scheme from Section 3.2 is applied to generate thrust arcs connecting the paths of the asteroids. The result of this automated procedure applied to the scenario where 8241 Agrius is the departure asteroid and 4138 Kalchas the target is illustrated in Fig. 2. The positions of closest relative distance are signified by the green spheres for 8241 Agrius and the red spheres for 4138 Kalchas, with the black arcs the converged rendezvous arcs and the black spheres the actual departure and arrival states.

The hybrid optimization process yields a single rendezvous segment connecting two asteroids and resulting in a trajectory arc with minimum propellant consumption for a specified thrust duration. The initial and terminal states along these arcs correspond to approximate asteroid positions and velocities from the CR3BP dynamic model such that the spacecraft is delivered from the vicinity of

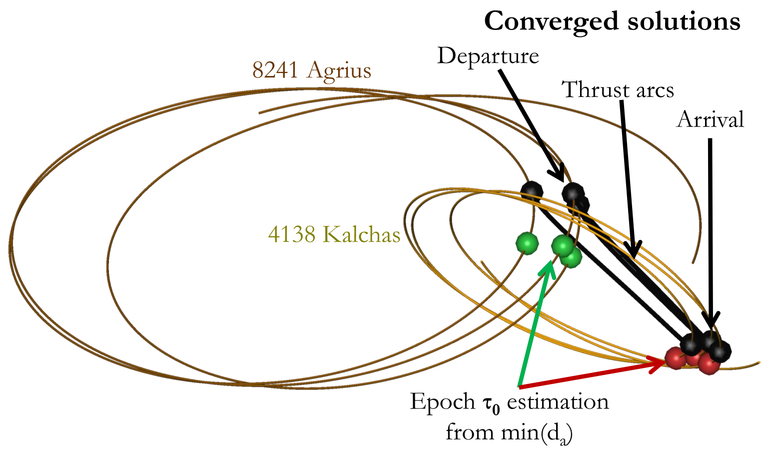

Figure 2. Initial guess of the rendezvous epochs for arcs from 8241 Agrius departure (green) to 4138 Kalchas arrival (red), with corresponding rendezvous arcs (black)

one asteroid to that of another. However, once a point solution is generated for a single specified thrust duration TD, a simple continuation scheme is applied that produces trajectory arcs over a large range of thrusting times. The continuation process updates the value of TD and uses the previously computed solution as the initial guess for the subsequent 2PBVP. The complete set of thrust arcs that is determined via the continuation scheme, termed a "family", represents a set of options for a single pre-determined asteroid-to-asteroid link within a design space relating engine operation time and propellant consumption for a spacecraft transfer. For this analysis, families of transfer arcs between any asteroid pair with thrust durations between $TD = 0.7$ and a nominal maximum $TD = 2.0$ in non-dimensional time units, or 483 to 1379 days, are produced. Some families do not cover the full range of thrust durations since the iteration process is terminated once the epoch expands to the limits of the window, i.e., Oct. 3, 2021 to Oct. 3, 2061. Note that for every thrust arc segment within these families, the initial spacecraft mass is assumed to be $m_0 = m_r = 500$kg, or $m_0 = 1$ non-dimensional units. (Of course, this initial mass may be adjusted in the tour construction process.) Once the independent solutions comprising the families of rendezvous arcs are computed, the initial conditions are stored for future use; this set of stored initial conditions is termed a "library".

4.2 Rendezvous Sequence Construction

To generate a potential tour sequence, an automated process extracts independent families of arcs from the library of solutions, selects individual rendezvous legs from within these families, and combines them into a series of thrust and coast segments. Since there are many possible thrust arcs across any given family, and the automatic procedure extracts only one solution arc per family, a trade-off is available between thrust duration TD, departure epoch τ_0, and arrival mass m_f. In general, m_f increases with TD while τ_0 decreases; however, it is observed that the quantity $(TD+\tau_0)$ usually increases with larger values of TD. For this investigation, the tour sequence algorithm allows one of three possible thrust duration options over all families in a potential sequence:

- Maximum TD, and therefore maximum m_f and arrival epoch with minimum τ_0,
- Minimum TD, with the reverse result,
- Median TD, with median values of arrival mass and departure and arrival epochs.

Once specific thurst arcs are selected, approximations are employed to estimate the performance metrics associated with a particular tour. For example, propellant consumption during each interval of engine operation must be incorporated into an equivalent cost corresponding to any potential tour scenario comprised of several rendezvous arc segments. Accordingly, for a rendezvous sequence built from n thrust intervals, the approximate propellant mass consumed m_{cons} is computed via

$$m_{consumed} = m_0 \left(1 - \prod_{i=1}^{n} \frac{m_i}{m_0} \right) \tag{26}$$

where m_i is the arrival mass in kilograms at the end of the i^{th} independently generated thrust arc.[1] For feasible options, this approximation can always be evaluated against a more rigorous model.

Since the families representing asteroid-asteroid transfer arcs are independently created, the selected rendezvous sequences must be evaluated to ensure they are physically realizable and satisfy mission constraints. Frequently, the two most common constraints in mission design are propellant mass and mission duration, i.e., a finite amount of mass is available and a limited opportunity usually exists for a timeline. Therefore, a maximum amount of propellant is available for activities within the swarm m_p and a maximum mission duration TOF is specified in the automated tour design scheme. Thus, for a tour to be feasible, the estimated propellant consumpiton, m_{cons}, must be less than m_p and the final rendezvous must occur before $\tau_d + TOF$ where τ_d is the epoch corresponding to Earth departure. Additionally, since the goal is survey options for missions to the Trojan asteroids, a further constraint is imposed, that is, the spacecraft cannot re-visit an asteroid after departure. Ultimately, the arc selection procedure is summarized by the following steps:

1. Select desired initial asteroid, asteroid arrival epoch, and thrust duration option, and specify m_p and TOF;
2. Retrieve from library all thrust arc families departing from current asteroid;
3. Remove families that return to previously visited asteroids;
4. For given TD option, eliminate all families with departure epochs prior to the current departure epoch or beyond the arrival epoch $\tau_d + TOF$;
5. Estimate spacecraft mass at end of all thrust arcs and remove families where $m_{cons} > m_p$;
6. For the remaining families, update tour information to include data from new arcs;
7. Repeat Steps 2-6 until the exploration of all possible tours is complete.

All Earth-to-asteroid outbound legs possess a pre-specified duration of 3.5 years, the Earth departure epoch τ_d is easily computed once an asteroid arrival epoch is selected. The result of the sequence construction procedure is a set of potential tours with estimated propellant mass consumption values less than m_p and with total time within the swarm that is less than $(TOF - 3.5)$ years. Performance metrics include propellant consumed, swarm tour duration, coast time in the vicinity of the asteroids, and the number of asteroid encounters; specific sequences of interest are then selected for further analysis.

[1] For the case of impulsive maneuvers, an equivalent total trajectory cost is $\Delta v_{tot} = \sum_{i=1}^{p} \Delta v_i$ where Δv_{tot} is the total impulsive Δv and Δv_i is the equivalent value for one maneuver.

4.3 Outbound Leg Computation and Higher-Fidelity Models

For a specific Trojan tour of interest, an Earth-to-swarm segment must be included such that the spacecraft rendezvous with the first asteroid in the tour occures prior to the defined asteroid arrival epoch. As stated in Section 3.2, this arc is enabled by the use of a hybrid propulsion scheme where an initial Earth-departure V_∞ is specified. Recall that the objective of the optimization procedure for this leg is the minimization of the initial spacecraft mass subject to the constraint that the mass upon asteroid arrival equals 500 kg. This phase of the trajectory design process is also automated by creating a library of pre-generated trajectory arcs. So, point solutions for locally optimal rendezvous arcs between Earth and each of the 10 sample asteriods are computed where the departure epoch τ_d occurs within the year 2018 and the spacecraft arrives in the vicinity of the asteroid swarm 3.5 years later in 2021. Thereafter, for any specific tour, the pre-computed departure epoch is adjusted by a integer multiple of the Earth-Jupiter synodic period, that is, 398.88 days, such that the spacecraft arrives at the initial asteroid only a short time in advance of the selected starting epoch for the asteroid tour. This adjusted value of τ_d, as well as the previously generated engine operation parameters, are then employed as the initial guess for a new local optimization cycle producing a hybrid propulsion arc originating at Earth and terminating at the asteroid swarm.

Transitioning any solution or design to an ephemeris model is a key step for validation of the results. Given a possible asteroid tour mission, the cost as well as timing estimates and engine operation histories are obtained using a corrections algorithm in the point mass ephemeris model from Section 2.2 Also, for the tour within the swarm, accurate propellant costs are determined by incorporating the propellant consumed along previous thrust arcs, rather than assuming each thrust arc to be independent. For example, after arrival in the swarm, the first rendezvous arc between asteroids consumes propellant mass such that the initial spacecraft mass is less than 500 kg at the initiation of the second thrust arc. Accordingly, the optimization problem for the second asteroid-to-asteroid rendezvous arc possesses an 'initial' spacecraft mass equal to the arrival mass at the end of the previous rendezvous segment. The propellant usage computation then continues throughout the tour in the swarm. The initial spacecraft mass at swarm arrival is still specified to be 500 kg and, therefore, the Earth-to-asteroid arc still targets an arrival mass of 500 kg. For this investigation, only the gravity of the Sun and Jupiter are incorporated in the point mass ephemeris model; the gravitational effect of other celestial bodies, e.g. the Earth and Mars, are assumed to be negligible, even along the outbound leg.

5. Sample Asteroid Tour Trajectories

The automated tour generation procedure is applied to two mission scenarios. Recall that an initial target asteroid, arrival epoch, propellant mass within the asteroid swarm, mission duration, and asteroid-to-asteroid thrust arc duration must all be specified. An appropriate initial asteroid arrival epoch is determined from a grid search across a window of several years, so this arrival epoch selection is completed as a separate step in the analysis. However, the remaining constraints for the two scenarios are defined as follows:

1. Initial asteroid: 1143 Odysseus, $m_p = 100$ kg, $TOF = 10$ years, thrust arcs of median TD;
2. Initial asteroid: 7152 Euneus, $m_p = 150$ kg, $TOF = 14$ years, thrust arcs of median TD.

Recall that the mission duration TOF includes a 3.5 year Earth-to-asteroid leg, so the time within the swarm for the two proposed mission scenarios are defined as 6.5 and 10.5 years, respectively. For both scenarios, a constraint on Earth departure velocity is specified as $V_\infty = 7.5$ km/sec. These constraints enable several potential tours for a specified arrival epoch, although only one is analyzed in each case.

5.1 Initial Asteroid 1143 Odysseus, 10 Year Mission

The creation of a specific end-to-end trajectory that satisfies the mission requirements while enabling rendezvous with several asteroids begins by determining an initial asteroid arrival epoch. Combining thrust arcs from various families, as detailed in Section 4.2, is applied over a 25-year window from October 3, 2021 to October 3, 2046. During each year, the total number of potential tours, as well as the number of asteroids encountered per tour, is recorded and plotted in Fig. 3. As is apparent in the figure, several years offer an initial epoch that enables tours that rendezvous with three asteroids. Selecting the year 2025, year 4 in Fig. 3, for further analysis, three potential tours reach only two asteroids and three rendezvous sequences encounter three asteroids. A three-asteroid sequence

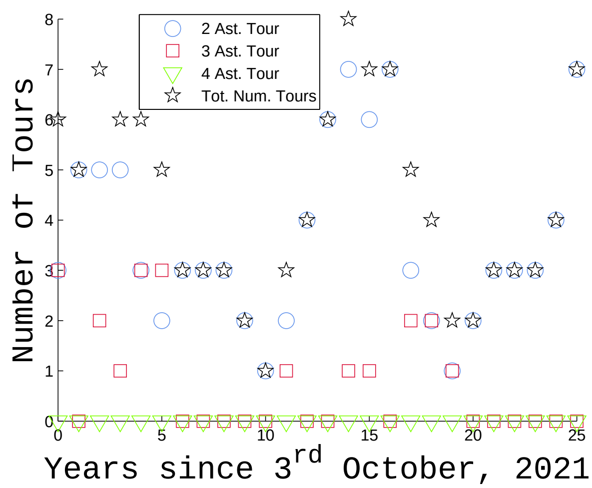

Figure 3. Potential tours originating at 1143 Odysseus and reaching a specified number of asteroids, in one-year increments, from Oct. 3, 2021.

reaching 4057 Demophon and 5012 Eurymedon is selected for further analysis. An outbound leg is determined, as described in Section 4.3; the estimated end-to-end costs as well as departure and arrival time histories are summarized in Tables 3 and 4. Note that the spacecraft mass at arrival at 1143 Odysseus is 500 kg, thus, 84.726 kg of propellant is expended on the outbound leg and 33.899 kg is consumed within the swarm. Thus, to complete the trajectory, roughly 20% of the spacecraft mass at Earth departure is propellant for the low-thrust engine. The remaining 66.101 kg of the mass budget that is available from m_p might enable extended missions and additional scientific instruments on the spacecraft. Additionally, the proposed trajectory allows approximately 5 months of operation in the vicinity of 1143 Odysseus and 7 months near 4057 Demophon before the final rendezvous with 5012 Eurymedon.

In addition to a mass budget and trajectory timeline, the physical path and engine operation histories are also of interest. Accordingly, the spacecraft trajectory under CR3BP dynamics is displayed in

Table 3. Spacecraft propellant budget for 10-year mission with tour of 3 asteroids

Quantity	Value		Units	CR3BP
	CR3BP	Ephemeris		Error (%)
Mass at Earth departure	584.726	583.238	kg	+0.255
Mass at final asteroid arrival	466.101	464.983	kg	+0.240
Total propellant consumption	118.625	118.251	kg	+0.316
V_∞ at Earth departure	7.50000	7.50000	km/sec	0

Table 4. Epochs of interest for 10-year mission with tour of 3 asteroids

Description	Gregorian Date YYYY:MM:DD:HH:MM:SS	
	CR3BP	Ephemeris
Earth departure	2021:6:3:13:0:27	2021:6:6:5:3:33
1143Odysseus arrival	2024:12:2:22:0:27	2024:12:5:14:3:33
1143Odysseus departure	2026:5:11:19:42:18	2026:3:30:3:43:18
4057Demophon arrival	2028:11:21:0:49:52	2028:10:9:8:50:53
4057Demophon departure	2029:6:28:7:56:47	2029:8:15:6:17:58
5012Eurymedon arrival	2031:12:11:22:56:58	2032:1:28:21:18:9

Fig. 4. The Earth-to-asteroid arc is magenta, arcs where the engine is operating within the swarm are dark gold, and coasts in the vicinity of asteroids are indicated by light blue. The position of the Earth is displayed at the Earth departure epoch of June 3, 2021. Note that upon arrival within the swarm, the thrust arcs are nearly planar, a fact that contributes to the relatively low propellant expenditure. Time histories of the thrust level and the engine I_{sp} are plotted in Fig. 5, where the Earth-to-1143 Odysseus segment is indicated in magenta, the 1143 Odysses to 4057 Demophon arc is green, and the 4057 Demophon to 5012 Eurymedon leg is red. As apparent in Fig. 5, the thrust and I_{sp} levels are consistent in magnitude over all periods of engine operation, that is, in the thrust range 10-50 mN and 5,000-20,000 sec that reflects I_{sp} values. With proper adjustments for spacecraft mass and timing, this tour can serve as a reference path for trajectory design with currently available constant specific impulse engines.

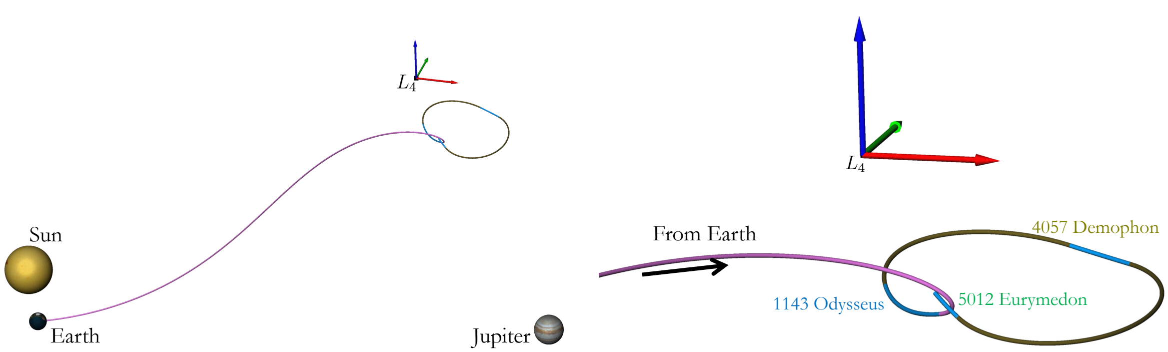

Figure 4. Plot of trajectory for tour with initial target 1143 Odysseus, outbound leg (pink), thrust arcs (gold), coasts in the vicinity of asteroids (blue), in Sun-Jupiter rotating frame.

The baseline design in the CR3BP that is generated by the automated procedure is now analyzed using higher fidelity motion for the Sun, Jupiter, and the target asteroids. All thrust arcs are

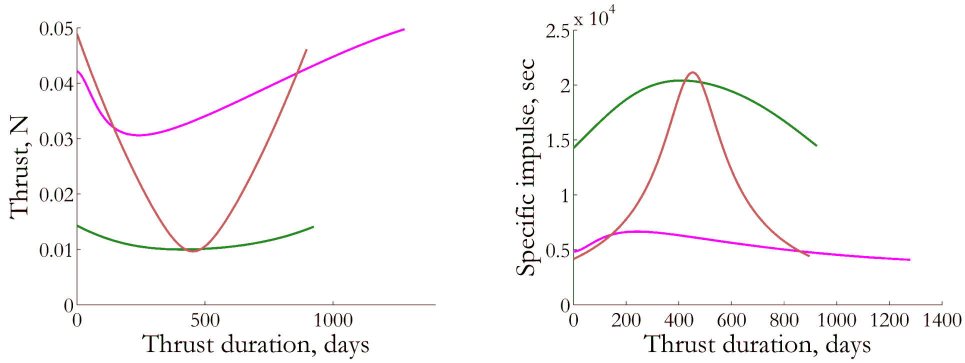

Figure 5. Thrust and I_{sp} profiles for outbound leg (pink) and first (green) and second (red) asteroid rendezvous arcs for mission scenario with initial asteroid 1143 Odysseus.

optimized using a Sun-Jupiter point-mass ephemeris model, where propellant consumed is retained from segment to segment. Thus, the initial mass of the spacecraft on the 4057 Demophon to 5012 Eurymedon leg is now the arrival mass of the spacecraft from the 1143 Odysseus to 4057 Demophon rendezvous arc. A target mass of 500 kg is retained for arrival at the initial tour asteroid, 1143 Odysseus. The results from the newly produced, higher fidelity tour are recorded in Tables 3 and 4, along with a percentage error in the propellant costs between the CR3BP and the point-mass ephemeris dynamics models. For this potential tour, the automated process accomplished in the simpler model over-estimates all reported masses, but by less than one percentage point in comparison with the higher-fidelity estimate. So, the required spacecraft mass at Earth departure is approximately 1.5 kg less than orginially estimated; the spacecraft mass upon arrival at 5012 Eurymedon is roughly 1 kg less than predicted. Overall, however, actual propellant consumed decreases by around 0.4 kg. The physical path of the spacecraft and the engine operation histories under the point-mass ephemeris model are very similar to those predicted by the automated CR3BP algorithm. The optimal departure and arrival epochs that are displayed in Table 4, however, can vary on the order of one to two months between the CR3BP and higher fidelity motion.

5.2 Initial Asteroid 7152 Euneus, 14 Year Mission

Repeating the trajectory design process for the second set of mission parameters further highlights the benefits of the automated procedure. For the same 25-year arrival epoch window, the swarm rendezvous arc combination procedure produces the results in Fig. 6. Now, with an increased propellant budget and an expanded time of flight, a greater number of potential mission scenarios are generated; many of these sequences result in encounters with up to four asteroids. For the arrival epoch corresponding to the year 2031, there are 29 feasible tours and, within that set, there are 8 sequences that link 4 asteroids. Select an asteroid tour originating at 7152 Euneus and possessing subsequent encounters with 5012 Eurymedon, 1143 Odysseus, and 5652 Amphimachus. An end-to-end trajectory is constructed with propellant costs and a timeline represented in terms of the epochs displayed in Tables 5 and 6. As before, the reference spacecraft mass is 500 kg upon swarm arrival, so 79.309 kg of propellant is consumed on the outbound segment while 118.985 kg is used within the asteroid-to-asteroid arcs. Of the swarm mass budget of 150 kg, 31.015 kg remains to enhance mission capabilities. For this mission scenario, approximately 34% of the spacecraft Earth departure mass must be propellant. As observed in Table 6, the spacecraft spends about 8, 17, and 5

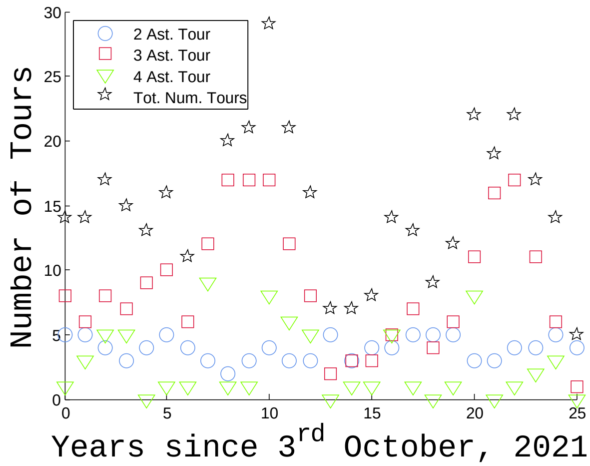

Figure 6. Potential tours originating at 7152 Euneus and reaching a specified number of asteroids, in one-year increments from Oct. 3, 2021.

months in the vicinity of 7152 Euneus, 5012 Eurymedon, and 1143 Odysseus, respectively, with an arrival at 5652 Amphimachus in September 2041.

Table 5. Spacecraft parameters for 14-year mission with tour of 4 asteroids

	Value			CR3BP
Quantity	**CR3BP**	**Ephemeris**	**Units**	**Error (%)**
Mass at Earth departure	579.309	584.795	kg	-0.938
Mass at final asteroid arrival	381.015	388.397	kg	-1.90
Total propellant consumed	198.294	196.397	kg	+0.966
V_∞ at Earth departure	7.50000	7.50000	km/sec	0

The trajectory generated by the automated procedure is displayed in Fig. 7, where the color scheme is consistent with Fig. 4. The position of the Earth is displayed at the Earth departure epoch of January 12, 2028. In contrast to the rendezvous trajectory that originates with 1143 Odysseus, the trajectories in this second scenarios are no longer nearly planar; thus, the propellant requirements are relatively higher. Time histories of thrust and engine I_{sp} values are plotted in Fig. 8, where the Earth to 7152 Euneus segment is magenta, and the first, second, and third asteroid-to-asteroid rendezvous arcs are green, red, and blue, respectively. As in the previous example, the thrust and I_{sp} levels are generally consistent over all periods of engine operation.

The potential 14-year tour is re-converged in the Sun-Jupiter point-mass ephemeris model, with the results displayed in Tables 5 and 6. For this case, the lower-fidelity predictions are no longer all over-estimates, with the CR3BP predicting lower Earth departure and 5652 Amphimachus arrival masses. As before, the CR3BP results over-predict the amount of propellant needed to complete the end-to-end trajectory. As is shown in Table 6, the predicted and actual departure and arrival epochs vary on the order of several months. Additionally, the physical path of the spacecraft in space and the engine operation time histories under ephemeris motion are similar to those illustrated in Figs. 7 and 8.

Table 6. Epochs of interest for 14-year mission with tour of 4 asteroids

Description	Gregorian Date YYYY:MM:DD:HH:MM:SS CR3BP	Ephemeris
Earth departure	2028:1:12:9:9:0	2028:1:12:16:21:35
7152Euneus arrival	2031:7:13:18:9:0	2031:7:14:1:21:35
7152Euneus departure	2032:3:4:14:1:45	2032:6:11:7:10:20
5012Eurymedon arrival	2034:9:14:19:9:20	2034:12:22:12:17:55
5012Eurymedon departure	2036:2:29:19:27:13	2035:12:30:6:23:11
1143Odysseus arrival	2038:9:11:0:34:48	2038:7:11:11:30:46
1143Odysseus departure	2039:2:22:2:22:19	2039:2:19:7:46:30
5652Amphimachus arrival	2041:9:3:7:29:54	2041:8:31:12:54:5

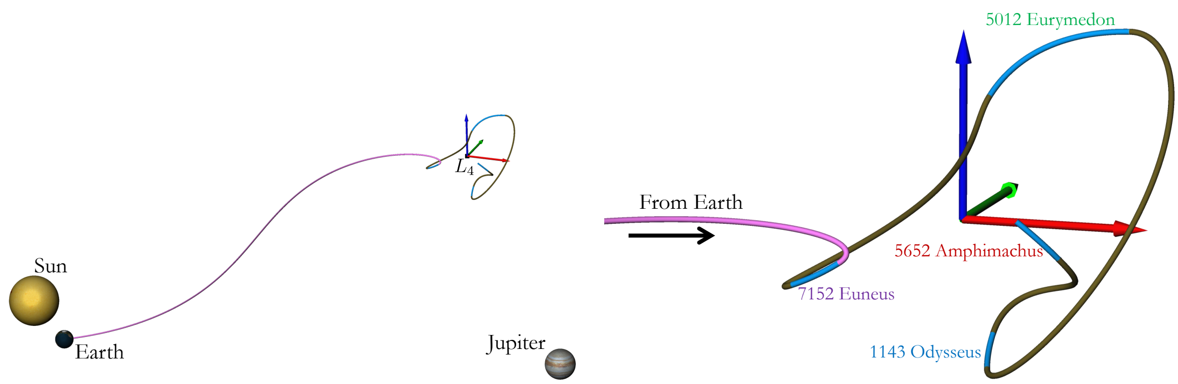

Figure 7. Plot of trajectory for tour with initial target 7152 Euneus, outbound leg (pink), thrust arcs (dark gold), coasts in the vicinity of asteroids (blue), in Sun-Jupiter rotating frame.

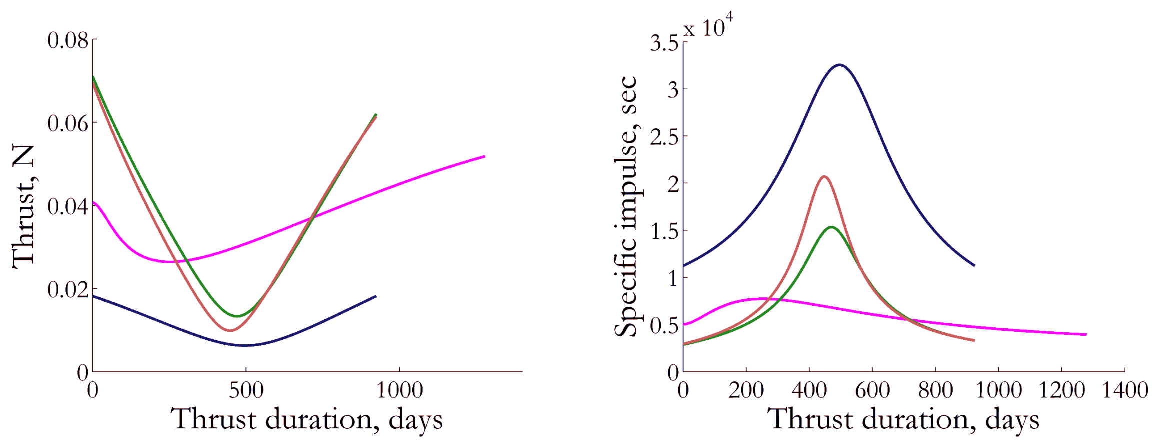

Figure 8. Thrust and I_{sp} profiles for outbound leg (pink) and first (green), second (red), and third (dark blue) asteroid rendezvous arcs for mission with initial asteroid 7152 Euneus.

6. Conclusions

An automated algorithm that generates potential trajectories, along with estimated propellant costs and other performance metrics, enabled by a variable specific impulse propulsion system has been developed and applied to the analysis of asteroid rendezvous tours within the Sun-Jupiter L_4 Trojan asteroid swarm. Indirect and direct optimization methods are blended to produce a hybrid optimization scheme. The optimization procedure is combined with an easily computed rendezvous detection criteria and employed to quickly and automatically yield a large number of rendezvous arcs between a selected set of asteroids. The independently generated asteroid-to-asteroid trajectory arcs are then rapidly sequenced into a series of thrust and coast arcs comprising several tour scenarios that satisfy a set of constraints on the trajectory. Individual tour sequences are then analyzed for propellant consumption, number of asteroids visited, and coast durations in the vicinity of the asteroids. A hybrid propulsion arc from the Earth to the asteroid swarm and consisting of an initial Earth departure velocity and a low-thrust arc is then adjoined to the inter-asteroid sequence. Baseline scenarios of particular interest are then optimized in a higher-fidelity model of motion and the accuracy of cost estimates from the automated scheme is assessed. For the sample tours examined, the automated algorithm yields fuel mass estimates within 2% of identical trajectories optimized from end-to-end in a Sun-Jupiter point-mass ephemeris model. In general, an Earth departure date is reliably predicted, while epochs of individual thrust arcs within the asteroid swarm vary on the order of a few months. Thus, the lower fidelity CR3BP offers accurate estimates of mission requirements while greatly reducing computational overhead. However, the procedure is not limited by dynamical regime and is readily extended to other mission architectures.

While the automated procedure provides cost and timing estimates for specific trajectories composing an asteroid tour mission, the algorithm also offers insight into overall mission planning. Of special advantage is the identification of favorable sequences of rendezvous arcs, where the procedure predicts a likely set of asteroids and a specific order of visitation, independent of the on-board propulsion system. Furthermore, families of thrust arcs computed using a variable specific impulse model can aid in the recognition of corresponding thrust durations that enable the use of constant specific impulse systems with a minimum of engine power cycles.

Several avenues are open for further investigation and refinement. In particular, higher fidelity modeling of celestial body motion will increase the accuracy of the resulting designs for both the asteroid-to-asteroid arcs as well as the end-to-end tour trajectory. Of particular importance is increased fidelity in the vicinity of the Earth-Moon region and of any near passages of other massive bodies, such as Mars. The automated procedure may be further enhanced to identify close passages and fly-bys of intermediate objects in the solar system, e.g. other asteroids within the swarm or along the outbound leg from Earth. A more sophisticated method of selecting individual thrust arcs from within families would also increase the versatility and power of the automated sequence generation. Furthermore, additional asteroids of interest may be included in the initial survey, and reliance on pre-computed libraries of solutions can be reduced or eliminated altogether. The inclusion of other low-thrust propulsion systems, e.g. constant specific impulse or power varying engines, will further increase the capability of the automated algorithm. Finally, the automated procedure may be applied to other scenarios requiring multiple low-thrust or hybrid propulsion arcs, whether as part of a baseline or an extended trajectory design.

7. Acknowledgements

This work was conducted at Purdue University and the Jet Propulsion Laboratory and is supported by the Purdue Research Foundation and a NASA Office of the Chief Technologist's Space Technology Research Fellowship, NASA Grant NNX12AM61H. Many thanks to Wayne Schlei, who helped immensely with the trajectory images, and Roby Wilson and the people of the Jet Propulsion Laboratory, Mission Design and Navigation Section.

8. References

[1] Augustine, N., Austin, W., Chyba, C., Kennel, C., Bejmuk, B., Crawley, E., Lyles, L., Chiao, L., Greason, J., and Ride, S. "Seeking a Human Spaceflight Program Worthy of a Great Nation." Tech. rep., U.S. Human Spaceflight Plans Committee, 2009.

[2] Brown, M. "Mission Concept Study: Trojan Tour Decadal Study." Tech. rep., National Aeronautics and Space Administration, 2011.

[3] Goebel, D., Brophy, J., Polk, J., Katz, I., and Anderson, J. "Variable Specific Impulse High Power Ion Thruster." "Joint Propulsion Conference," AIAA/ASME/SAE/ASEE, Tucson, Arizona, July 2005. Paper No. AIAA 2005-4246.

[4] Company, A. A. R. "VASIMR Technology." Accessed: November 28, 2010.

[5] Komurasaki, K., Arakawa, Y., and Takegahara, H. "An Overview of Electric and Advanced Propulsion Activities in Japan." "Proceedings of Third International Conference of Spacecraft Propulsion," pp. 27–39. Cannes, France, October 2000.

[6] Volle, M. "Optimal Variable-Specific-Impulse Rendezvous Trajectories Between Halo Orbits." "International Symposium on Space Flight Dynamics," Japan Society for Aeronautical and Space Sciences and ISTS, Kanazawa, Japan, June 2006. Paper No. ISTS 2006-d-73.

[7] Russell, R. "Primer Vector Theory Applied to Global Low-Thrust Trade Studies." Journal of Guidance, Control, and Dynamics, Vol. 30, No. 2, pp. 460–473, March-April 2007.

[8] Senent, J., Ocampo, C., and Capella, A. "Low-Thrust Variable-Specific-Impulse Transfers and Guidance to Unstable Periodic Orbits." Journal of Guidance, Control, and Dynamics, Vol. 28, No. 2, pp. 280–290, March-April 2005.

[9] Mingotti, G., Topputo, F., and Bernelli-Zazzera, F. "Combined Optimal Low-Thrust and Stable-Manifold Trajectories to the Earth-Moon Halo Orbits." New Trends in Astrodynamics and Applications III, Vol. 886, No. 2, pp. 100–112, February 2007.

[10] Martin, C. and Conway, B. "Optimal Low-Thrust/Invariant Manifold Earth Moon Transfer Trajectories." "Space Flight Mechanics Meeting," AAS/AIAA, San Diego, California, February 2010. Paper No. AAS 10-105.

[11] Betts, J. "Survey of Numerical Methods for Trajectory Optimization." Journal of Guidance, Control, and Dynamics, Vol. 21, No. 2, pp. 193–207, March-April 1998.

[12] Bryson, A. E., Jr. and Ho, Y.-C. Applied Optimal Control. Blaisdell Publishing, Waltham, Massachusetts, 1969.

[13] Gill, P. E., Murray, W., and Saunders, M. A. "SNOPT: An SQP algorithm for large-scale constrained optimization." Society for Industrial and Applied Mathematics Journal of Optimization, Vol. 12, pp. 979–1006, 2002.

[14] Izzo, D., Vinkó, T., Bombardelli, C., Brendelberger, S., and Centuori, S. "Automated Asteroid Selection for a 'Grand Tour' Mission." "58th International Astronautical Congress," Hyderabad, India, September 24-28 2007. Paper No. IAC-07-C1.7.07.

[15] Canalias, E., Mithra, A., and Carbonne, D. "End-to-End Trajectory Design for a Chemical Mission Including Multiple Flybys of Jovian Trojan Asteroids." "AAS/AIAA Astrodynamics Specialist Conference," Girdwood, Alaska, July 31 - August 4 2011. Paper No. AAS 11-481.

[16] Solar System Dynamics Group. HORIZONS System. Jet Propulsion Laboratory. http://ssd.jpl.nasa.gov/?horizons.

[17] Keller, H. B. Numerical Solution of Two Point Boundary Value Problems. Society for Industrial and Applied Mathematics, Philadelphia, Pennsylvania, 1976.